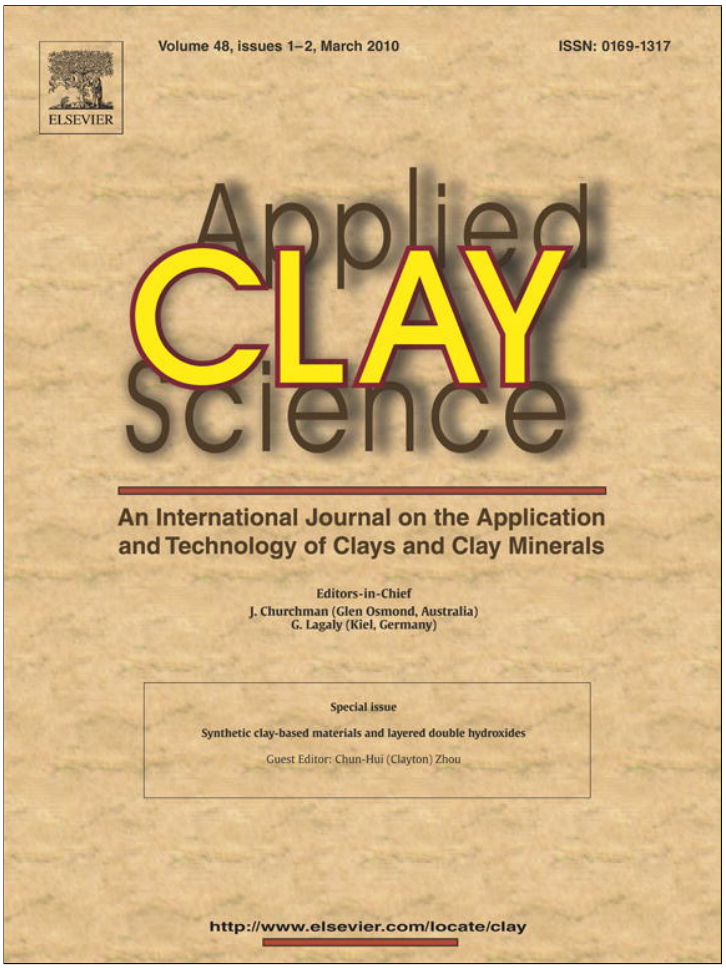

Applied Clay Science 48 (2010) 73–80

Contents lists available at ScienceDirect

Applied Clay Science

journal homepage: www.elsevier.com/locate/clay

Nonisothermal order–disorder phase transition of alkylammonium ions in nanoconfined space

Masaki Kajino [a], Tomotaka Saito [a,b], Masami Okamoto [a,*], Harumi Sato [c], Yukihiro Ozaki [c]

[a] Advanced Polymeric Nanostructured Materials Engineering, Graduate School of Engineering, Toyota Technological Institute, Hisakata 2-12-1, Tempaku, Nagoya 468-8511, Japan
[b] Research Laboratories, Toyota Boshoku Co., Toyoda-cho 1-1, Kariya 448-8651, Japan
[c] Department of Chemistry, School of Science and Technology, Kwansei-Gakuin University, Research Center for Environment Friendly Polymers, Sanda 669-1337, Japan

ARTICLE INFO

Article history:
Accepted 18 November 2009
Available online 27 November 2009

Keywords:
Order–disorder transition
Cationic surfactant
Nanoconfined space
Organo-montmorillonite

ABSTRACT

To understand the effect of confined space (interlayer space in montmorillonite (MMT)) on the nonisothermal ordering transition (chain packing) kinetics and disorder transition (chain melting) behavior including the conformational changes of the chain segment of the cationic surfactants, we have characterized MMT modified with dioctadecyl dimethylammonium ($DC_{18}DM$) ions (MMT-$DC_{18}DM$) using temperature-modulated differential scanning calorimeter (TMDSC), wide-angle X-ray diffraction (WAXD) and Fourier transform infrared spectroscopy (FTIR) techniques. For MMT-$DC_{18}DM$, the chain conformational disorder–order phase transition took place during the cooling process. The transition peak was much broader and it appeared at lower temperature (T_c) when compared to the crystallized dioctadecyl dimethylammonium bromide ($DC_{18}DM$-Br), as a reference.

In MMT-$DC_{18}DM$, the formation of gauche conformers was enhanced and the chains were not as densely packed as in crystalline $DC_{18}DM$-Br. The normal crystallization took place in the bulk during the nonisothermal crystallization of $DC_{18}DM$-Br. The confined ions ($DC_{18}DMs$) in one or two dimensional order contributed to the nonisothermal chain packing for a higher cooling rate of 5.0–20.0 °C/min. The observed chain packing in confined space at different T_c ranges (cooling rate >5.0 °C/min) could be explained by much lower energy barrier.

1. Introduction

Over the last few years, the utility of inorganic nanoscale particles as filler to enhance the polymer performance has been established. Of particular interest is the recently developed nanocomposite technology consisting of a polymer and organically modified layered silicate (organo-clay) because they often exhibit remarkably improved mechanical and various other material properties when compared to those of virgin polymer or conventional composite (micro/macro-composites) (Sinha Ray and Okamoto, 2003; Gao, 2004; Okada and Usuki, 2006; Hussain et al., 2006). The nanocomposites and their self-assembly behavior have recently been approached to produce nanoscale polymeric materials (Vaia and Wagner, 2004). Additionally, these nanocomposites have been proposed as model systems to examine polymer structure and dynamics in confined environments (Krishnamoorti et al., 1996; Vaia and Giannelis, 1997a; Rao and Pochan, 2007).

The self-assembly and dynamics of the cationic surfactants intercalated in montmorillonite (MMT) (Vaia et al., 1994; Vaia and Giannelis, 1997b; Osman et al., 2000; Osman et al., 2002; Li and Ishida, 2002, 2003; Osman et al., 2004; Lagaly et al., 2006; Heinz et al., 2008) have been extensively investigated as well as molecular simulations (Heinz et al., 2005; He et al., 2005; Heinz et al., 2006, 2007, 2008). The conformational disorder in the alkyl chains on MMT surfaces has been reported by Vaia et al. (1994) as revealed by Fourier transform infrared (FTIR) spectroscopy. Li and Ishida (2002, 2003) and Osman et al. (2002, 2004) reported the chain conformational order–disorder transition of the cationic surfactant in MMT galleries. At low temperature (~20 °C) the alkyl chains preferentially are in all-trans conformation. The conformational transition of the chains takes place with increasing temperature, leading to a disordered phase (at 60 °C), where the chains assume a random conformation. The observation of the phase transitions upon heating, variable chain conformation and metastable phases has been extensively investigated. The molecular simulations have helped to understand the molecular-level structure, chain conformation, tilt angle of the alkyl chains and the phase transitions. Heinz et al. (2003) reported that about 4 out of 16 torsion angles were gauche in octadecyl trimethylammonium ions on mica surfaces (C_{18}-mica) at 20 °C, whereas the number of gauche-bonds was increased to 5 at 100 °C. The number of gauche-bonds remains steady with further increasing temperature. Assuming a homogeneous coverage of the entire surface area, the average molecular axis of the octadecyl trimethylammonium ions was inclined relative to the

* Corresponding author.
E-mail address: okamoto@toyota-ti.ac.jp (M. Okamoto).

0169-1317/$ – see front matter © 2009 Elsevier B.V. All rights reserved.
doi:10.1016/j.clay.2009.11.025

mica surface normal in the angles of 55° ± 2°. This value well agrees with experimental data (Nuzzo et al., 1990; Binder et al., 1998; Brovelli et al., 1999). The simulation exhibited a major conformational change due to melting of the alkyl chains and an increased mobility of the C_{18}-ions across the surface cavities at elevated temperature. Brovelli et al. (1999) discussed the experimentally observed two distinct phase transitions on heating. The first transition at 40 °C was due to breaking of the disordered C_{18} chains in the island structure (Fujii et al., 1999) and the second transition at 60 °C was due to rearrangements of the C_{18}-ions on the surface. The concept packing density λ (≅A_C/A_S) (surface saturation), which is given by the average cross-sectional area of an alkyl chain A_C in relation to the available surface area A_S, and its relation to conformational order were used to understand the behavior of alkyl chains on the surface (Heinz et al., 2003; Heinz et al., 2008). They reported a simple relation between λ and the tilt angle θ for homogeneous layers is given by λ = cos θ.

The geometric parameter λ determines the preferred self-assembly structure into the MMT interlayer spaces. For MMT, A_S, is 1.404 nm^2 with layer charge of 0.333 (Yoshida and Okamoto, 2006a; Heinz et al., 2008). The cross section of all-trans alkyl chains perpendicular to its axis is $A_{C,\,trans}$ = 0.188 nm^2 reported in the literature (Yoshida and Okamoto, 2006a; Heinz et al., 2008). The λ value of C_{18}-MMT is low (~0.13). At low λ (<0.2) the alkyl chains are oriented parallel to the MMT surface having a layer-by-layer structure, which leads to a high degree of conformational disorder and no reversible order–disorder transitions. At an intermediate packing density (0.2<λ<0.75), alkyl chains adopt orientations with segmental tilt angles in the range from 78° to 42°. The chain conformations are between liquid-like and crystalline. This simple model is independent of the alkyl chain length, the chemical nature of the surface and of the cationic surfactant head group.

Despite extensive studies, the relation between packing density and chain dynamics under ordering transition is still sparse. Therefore, in this paper, we aim to confirm the nonisothermal disorder–order phase transition (chain packing) kinetics and disorder transition (chain melting) behaviors including the conformational changes of the chain segment of the alkyl chains in confined space (nano-gallery space of the layered fillers). Knowledge of such investigations shall be useful in assessing how does the phase transitions appear to be fundamentally different from those observed in bulk.

2. Experimental part

2.1. Materials

OMLF used in this study was montmorillonite (MMT) (cation exchange capacity (CEC) of 90 meq/100 g, average length of 150–200 nm) intercalated with dioctadecyl dimethylammonium ($DC_{18}DM$) ions by ion exchange reaction (Yoshida and Okamoto, 2006a), which will be hereafter defined as MMT-$DC_{18}DM$. The loading amount of the $DC_{18}DM$ cations, which was calculated from thermogravimetric analysis (TGA) was 29.5 wt.% (Yoshida and Okamoto, 2006a). The overall degree of ion exchange was about 89%. The surface charge density is particularly important because it determines the interlayer structure of cationic surfactants as well as CEC. The characterizing method consists of total elemental analysis and the dimension of the unit cell (Yoshida and Okamoto, 2006a):

$$\textit{Surface charge}: e^- / nm^2 = \zeta / ab \quad (1)$$

where ζ is the layer charge (0.33 relative cation density for MMT; Bailey, 1988). a and b are cell parameters of MMT (a = 5.18 Å, b = 9.00 Å; Yoshida and Okamoto, 2006a). About 90% of the interlayer Na^+ ions are replaced quantitatively by cationic surfactants (Yoshida and Okamoto, 2006a). The characteristic parameters of the nano-fillers are also summarized in Table 1. From these results, we can estimate the surface area per charge A_S, which is calculated to be 1.41 nm^2 for MMT. This estimation assumes that the cations are evenly distributed in a cubic array over the nano-filler surface and that half of the cations are located on the one side of the platelet and the other half reside on the other side. As reported by Heinz et al. (2008), in the present study, the calculated λ value of MMT-$DC_{18}DM$ is ~0.27, corresponding to the intermediate packing density.

Table 1
Characteristic parameters of montmorillonite (MMT).

Parameters	MMT
Chemical formula	$Na_{0.33}(Al_{1.67}Mg_{0.33})\ Si_4O_{10}(OH)_2$
Particle size[a]/nm	~100–200
BET area/m^2/g	~700
CEC[b]/meq/100 g	~90(90)
Area per charge/nm^2	1.41
Density/g/cm^3	2.50
Refractive index ($n^{20}{}_D$)	1.55
pH	7.5–10

[a] Yoshida and Okamoto, 2006b.
[b] Methylene blue adsorption method. The values in the parenthesis are calculated from chemical formula of nano-fillers.

For comparison, dioctadecyl dimethylammonium bromide ($DC_{18}DM$-Br), purchased from Aldrich, was used as a reference.

2.2. Characterization methods

The specimens were characterized by using temperature-modulated differential scanning calorimeter (TMDSC) (TA 2920; TA Instruments) under nitrogen at a heating and cooling rate of 5 °C/min with a heating/cooling cycle of the modulation period of 60 s for an amplitude of +/−0.769 °C. The chain packing and/or crystallization temperature with cooling from melt (T_c), the melting temperature (T_m) and heat of fusion (ΔH), were calibrated with Indium before experiments.

WAXD analyses were performed using an Mxlabo X-ray diffractometer (MAC Science Co.; 3 kW, graphite monochromator, CuKα radiation (λ_x = 0.154 nm), operated at 40 kV and 20 mA). Samples were scanned in fixed time mode with counting time of 2 s at room temperature under a diffraction angle (2Θ) in the range of 1° to 70°.

The crystalline texture of $DC_{18}DM$-Br during the cooling process from melt state (~100 °C) was also measured. The thin samples were crystallized on the Linkam hot stage mounted on a polarized optical microscope (POM) (Nikon OPTI-PHOTO2-POL). After the complete crystallization, the samples were observed using POM and fitted with a color-sensitive plate to determine the sign of birefringence, and the photographs were taken. The details regarding POM observation can be found in our previous paper (Kubo et al., 1998).

Fourier transform infrared (FTIR) spectra were collected at 2 cm^{-1} nominal resolution using a Varian FTS7000 spectrometer equipped with a MCT detector in transmission mode. The spectra were obtained by averaging 32 scans with a mean collection length of 1 s per spectrum. The background spectra used for reduction were collected at the same temperature (T) range of 25–120 °C for $DC_{18}DM$-Br and 25–80 °C for MMT-$DC_{18}DM$, respectively, with the samples. The homogenous mixture of KBr powder and $DC_{18}DM$-Br (fine powder) or MMT-$DC_{18}DM$. (powder) in the weight ratio 98:2 was prepared. The mixtures were made into pellets having a thickness of ~400 μm, placed in a homemade heating chamber and heated up to a temperature T with a heating/cooling rate of 200–300 °C/min. The collected data was processed with Grams/AI® software (Thermo Galactic Co., USA).

3. Results and discussion

3.1. DSC scan and crystalline structure

Fig. 1 shows the TMDSC thermograms of MMT-$DC_{18}DM$ and $DC_{18}DM$-Br from −50 °C to melt, cooling from molten state (~100–120 °C) and

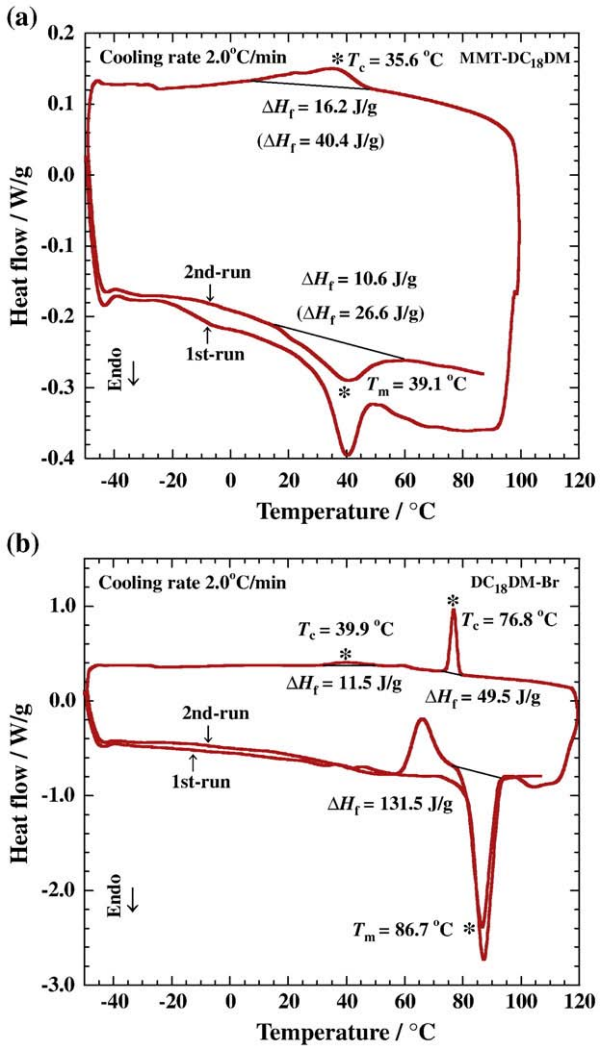

Fig. 1. TMDSC scans for (a) MMT-DC_{18}DM and (b) DC_{18}DM-Br. The total endothermic and exothermic heat flows in the parenthesis indicate the total heat flows for 100% cationic surfactant.

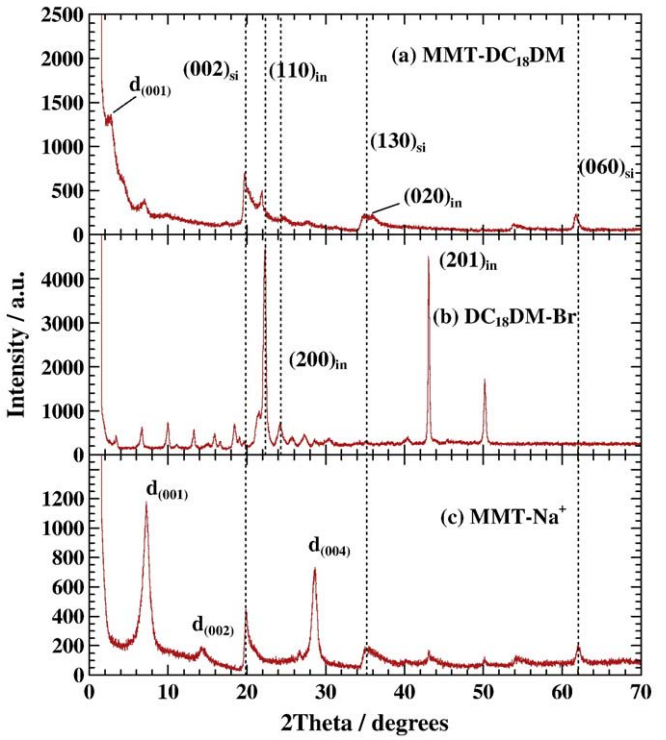

Fig. 2. Typical WAXD profiles of (a) MMT-DC_{18}DM, (b) DC_{18}DM-Br and (c) pristine MMT (MMT-Na^+).

2nd heating at a rate of 2.0 °C/min. For DC_{18}DM-Br, the formation of the maximum crystallization peak was obtained at 76.84 °C, accompanied with a small peak at 39.69 °C. For MMT-DC_{18}DM, the peak was much broader (35.55 °C) due to the disorder–order phase transition (chain packing) in the confined space (Osman et al., 2004; Heinz et al., 2008, 2003). Both chain packing temperatures (T_c) for MMT-DC_{18}DM and crystallization temperature (T_c) from melt state for DC_{18}DM-Br sensitively depended on the cooling rate. A large shift was observed at chain melting point (T_m = 39.14 °C) and endothermic/exothermic heat behavior of MMT-DC_{18}DM (ΔH_f) when compared to the T_m of DC_{18}DM-Br crystals (86.66 °C). The depression of T_m in MMT-DC_{18}DM increased due to the thermal stability of the ordered structure, formed during the cooling process. The enthalpy of phase transition was 20% of the enthalpy of melting of DC_{18}DM-Br, which implied the breakage of the disordered alkyl chain structure. This speculation is in accord with the results reported by Heinz et al. (2003).

The crystal structures of MMT-DC_{18}DM and DC_{18}DM-Br were analyzed by WAXD as shown in Fig. 2. The diffraction pattern of pristine MMT (MMT-Na^+) was taken as the reference to compare with the diffraction peaks of silicate layer.

In Fig. 2 (a), the mean basal spacing of the (001) plane ($d_{(001)}$) is 3.572 nm ($2\theta = 2.47$). The interlayer distance was 2.653 nm, estimated by subtracting the value of layer thickness (0.919 nm) of MMT (Heinz et al., 2007). This is an important point for the following discussion on the interlayer structure.

The molecular dimensions of various cationic surfactants were proposed by using a molecular dynamics program (MM2 in Quantum CAChe, Fujitsu Ltd.), by taking van der Waals radii into consideration. The structure optimization was based on minimization of the total energy of the molecular system. The calculated models of the cationic surfactant structures were presented in our previous paper (Yoshida and Okamoto, 2006a). For the DC_{18}DM cation molecule, the length, thickness and width were 2.601, 0.372 and 0.372 nm respectively with an all-trans conformation. Since the length of the alkyl unit is more than 2 nm, the spacing (distance between exchange sites) of 1.188 nm does not allow the parallel layer arrangement of flat-lying chains (Li and Ishida, 2002; Heinz et al., 2008) in the MMT nano-galleries.

The WAXD analysis coupled with an all-trans conformation of the cationic surfactant can assume that the alkyl chains radiate away from the surface forming a one-layer extended paraffin type structure (Lagaly, 1970) without tilting to the silicate layers when we compared to the molecular modeling of the interlayer distance.

WAXD profiles of crystallized DC_{18}DM-Br during cooling process (see Fig. 1 (b)) from molten state (~120 °C) in Fig. 2 (b) and the corresponding POM image are shown in Fig. 3. The crystalline texture of DC_{18}DM-Br was evolved quickly during the cooling process. The assignment of the reflections associated with the crystalline structure was based on the orthorhombic unit cell (space group *Pnam*: $a = 0.741$ nm, $b = 0.495$ nm and $c = 0.255$ nm) and chain configurations (Bunn, 1939). The reflections at $2\theta = 22.36°$, 24.11° and 42.97°- correspond to $(110)_{in}$, $(200)_{in}$ and $(201)_{in}$ planes of the crystallite, respectively. For MMT-DC_{18}DM, these reflections are observed as small peaks except the evolution of $(201)_{in}$. The peak occurring from the $(110)_{in}$ plane (parallel to the alkyl chains) is shifted towards the lower reflection angle and another reflection peak at $2\theta = 36°$ (assigned to the reflection of $(020)_{in}$ plane) appears. The large inter-chain distances may be due to the formation of poor chain packing in the confined space.

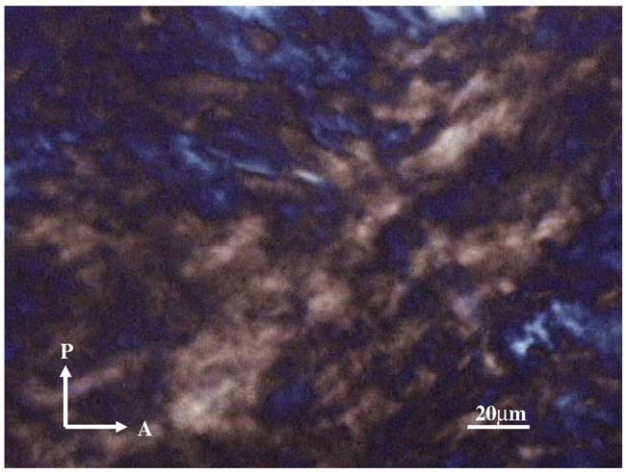

Fig. 3. Polarized optical micrograph for crystallized $DC_{18}DM$-Br during the cooling process.

In Fig. 2 (c), the reflections at $2\theta = 19.83°$, 35.38° and 62.02° correspond to the planes $(002)_{si}$, $(130)_{si}$ and $(060)_{si}$ of the crystalline silicate lattice, respectively (Okamoto et al., 2000). These reflections were clearly observed in Fig. 2 (a).

3.2. Temperature dependence of ordered structure development

The temperature dependence of WAXD profiles of MMT-$DC_{18}DM$ with heating and cooling processes is shown in Fig. 4. With increasing temperature the intensities from $(110)_{in}$ to $(200)_{in}$ gradually decreases without any peak shifts. The reflection from the $(200)_{in}$ plane vanishes at around 60 °C and above. These features were summarized in the plot of intensity ratio against temperature. The intensity from the $(002)_{si}$ plane was taken as a reference. The ratio of $I(110)_{in}/I(002)_{si}$, related to the chain melting (heating process) and chain packing (cooling process) of the alkyl chains into the MMT galleries, rapidly decreased with temperature beyond 40 °C (corresponding to T_m [see Fig. 1 (a)]), and finally reached a constant value (~0.635). On cooling from melt (~80 °C) the same phenomena were observed too, which can be termed as a reversible process. The ratio of $I(200)_{in}/I(002)_{si}$ showed a gradual decrease with temperature from the very beginning of the heating. Compared to the heating process, the intensity ratio under the cooling process is slightly lower and there is a hysteresis phenomenon.

On the other hand, through cyclic thermal treatment the interlayer spacing $d_{(001)}$ remained constant, whereas the intensity was found to be more sensitive to temperature. The intensity ratio of $I(001)_{MMT\text{-}DC18DM}/I(002)_{si}$ under the cooling process showed a slightly higher value than that of the heating process. This feature seems to be a reversible process with some hysteresis.

FTIR spectroscopy was used to probe the conformational change and lateral chain–chain interaction. The frequency, width and intensity of the asymmetric ($\nu_{as}(CH_2)$) and symmetric ($\nu_s(CH_2)$) methylene stretching bands near 2920 and 2851 cm^{-1}, respectively, were sensitive to the gauche/trans conformer ratio. For example, in the melting of nonadecane, on going from the crystalline phase (all-trans conformation) to a disordered liquid state rich in gauche population, ($\nu_{as}(CH_2)$) and ($\nu_s(CH_2)$) were shifted from 2916 to 2923 cm^{-1} and from 2848 to 2853 cm^{-1}, respectively (Osman et al., 2000). The similar shifts to higher frequencies were observed in both MMT-$DC_{18}DM$ and $DC_{18}DM$-Br on heating across the transition temperatures ($=T_m$) detected by TMDSC (Fig. 1), suggesting the conformational changes in alkyl chains. For MMT-$DC_{18}DM$, a band of ($\nu_{as}(CH_2)$) exhibited higher frequency (2921.1 cm^{-1}) than that of $DC_{18}DM$-Br (2919.2 cm^{-1}), suggesting a higher population of the gauche conformers. The temperature dependence of the bandwidth (full width at half-maximum: FWHM) is shown in Fig. 5. The bandwidth is closely proportional to the degree of molecular mobility. For MMT-$DC_{18}DM$, at 25 °C, the bandwidths at both characteristic bands ($\nu_{as}(CH_2)$) and ($\nu_s(CH_2)$) were wider than those of $DC_{18}DM$-Br, whereas its variation with increasing temperature exhibited narrow values (4 cm^{-1} for ($\nu_{as}(CH_2)$) and 5 cm^{-1} for ($\nu_s(CH_2)$), respectively) when compared with those of $DC_{18}DM$-Br (11 cm^{-1} for ($\nu_{as}(CH_2)$) and 7 cm^{-1} for ($\nu_s(CH_2)$)). These results conclude the formation of enhanced gauche conformers and the poor chain packing of the ordered alkyl chains in MMT-$DC_{18}DM$ when compared to the crystallized $DC_{18}DM$-Br. Upon heating, the mobility of the alkyl chains is enhanced owing to the chain melting in the confined space. The alkyl chains are tethered to the silicate surface on one end and the translational freedom of the chains is limited due to the ion–dipole interaction between the head group of $N^+(CH_3)_2$ and silicate surface. In addition, as reported in our previous paper (Yoshida and Okamoto, 2006a, b), the pressure drop (Δp) into the nano-galleries, which makes the chain mobility more difficult, is also an important parameter. The estimated pressure difference (≈24 MPa) was much larger than the atmospheric pressure (~0.1 MPa). For these reasons, another interesting feature related with the confined alkyl chains is shown in Fig. 5. For $DC_{18}DM$-Br, the sharp changes in peak maxima and FWHM were seen around the T_m of the crystallized alkyl chains (indicated with dashed lines of Fig. 5) in the bulk. On the other hand, for MMT-$DC_{18}DM$, the confinement effects lead to a more steady increase up to 80 °C.

Fig. 6 shows the comparison of the characteristic band ($\nu_{as}(CH_2)$) for heating and cooling processes. For MMT-$DC_{18}DM$ and $DC_{18}DM$-Br, the hysteresis phenomena were observed in both cases, i.e. the peak maxima in the cooling process exhibit higher frequency when

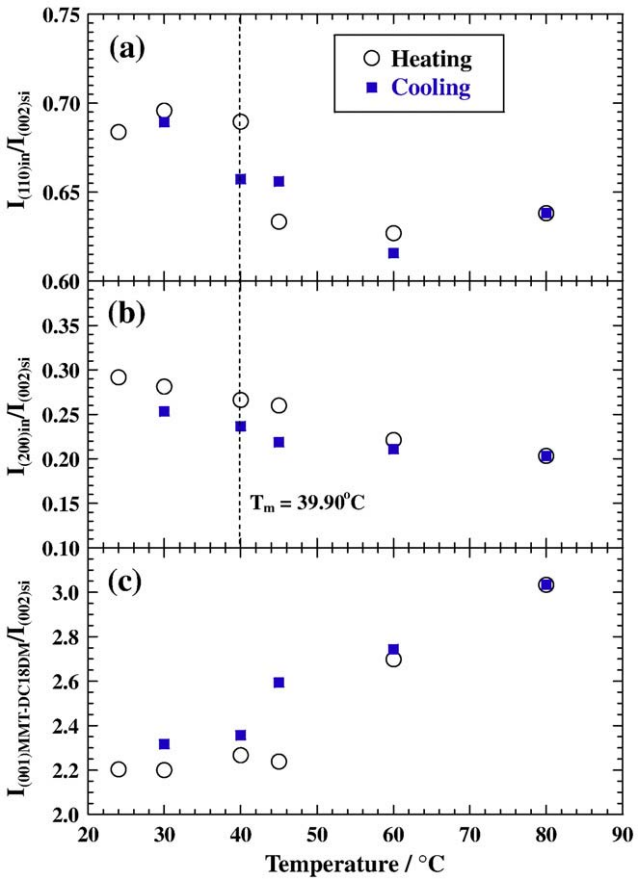

Fig. 4. Temperature dependence of characteristic intensity ratios of (a) $I(110)_{in}/I(002)_{si}$, (b) $I(200)_{in}/I(002)_{si}$ and (c) $I(001)_{MMT\text{-}DC18DM}/I(002)_{si}$ with heating and cooling processes. The dashed line indicates T_m detected by TMDSC.

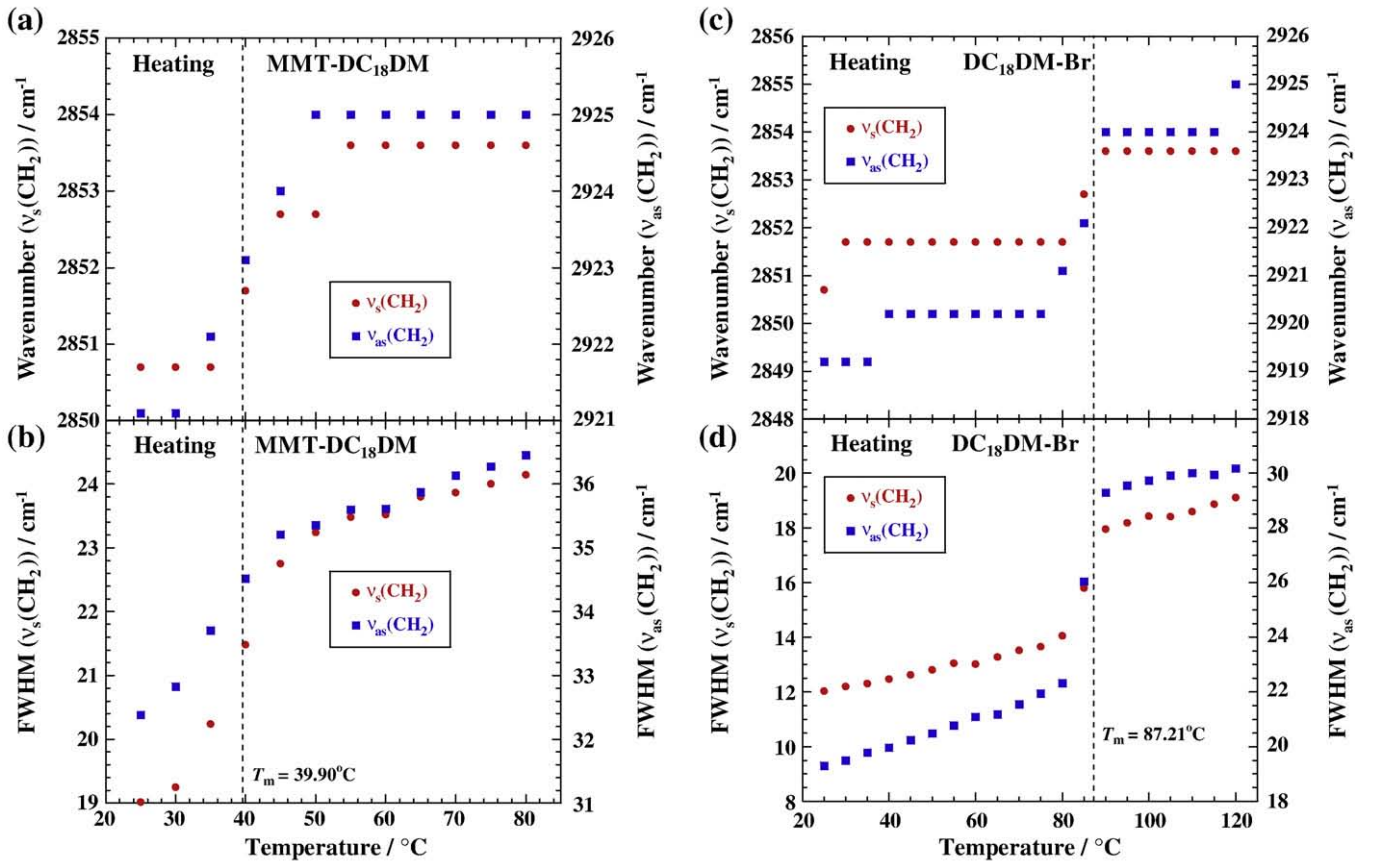

Fig. 5. Temperature variations of frequency shifts and FWHM for heating process for MMT-DC_{18}DM ((a) and (b)), and DC_{18}DM-Br ((c) and (d)). The dashed line indicates T_m detected by TMDSC.

compared to the heating process owing to the difference between T_m and T_c (indicated with dashed lines of Fig. 6). For the variation of FWHM, the same trend was found in both systems (Fig. 7). This means that the temperature dependence of the conformational changes and the mobility of the alkyl chains agrees well with the thermal transition temperatures as revealed by TMDSC.

3.3. Ordering kinetics and crystallization kinetics

To understand the disorder–order phase transition kinetics of the alkyl chains in MMT-DC_{18}DM, a differential scanning calorimeter was used to estimate the overall transitions under nonisothermal process. The broadening of the crystallization peak occurred with increase of cooling rate in the bulk crystallization of DC_{18}DM-Br. On the other hand, in MMT-DC_{18}DM, the chain packing peak profile remained the same with the increase of cooling rate. The effect of confined molecules (DC_{18}DMs) on the nonisothermal phase transition can be detected from this analysis. Fig. 8 shows the cooling rate dependence of T_c and ΔH_f. For MMT-DC_{18}DM, T_c value showed a gradual decrease with the cooling rate (increasing up to 5 °C/min), beyond which the temperature rapidly decreased with the rapid decrease in ΔH_f. On the other hand, the DC_{18}DM-Br T_c decreased steadily up to 20 °C/min and ΔH_f first stood almost constant (~46 J/g), later increased steadily, implying the occurrence of normal crystallization in the bulk. Thus, the crystallization is controlled by the degree of the supercooling ($\equiv T_m - T_c$), such as the polymer melt crystallization (Asai et al., 2008). We can conclude that the phase transition in the confined space is more obvious as opposed to the bulk crystallization.

Fig. 9 shows the time variation of the relative degree of the ordering during phase transition ($\Delta H_f(t)/\Delta H_f(\text{total})$). This was calculated from the ratio area of the exotherms up to time (t) divided by the total exotherm area, i.e.:

$$\Delta H_f(t) / \Delta H_f(\text{total}) = \frac{\int_{t_0}^{t} (dH_f / dt) dt}{\int_{t_0}^{\infty} (dH_f / dt) dt} \quad (2)$$

where (dH_f/dt) is the heat flow rate and t_0 is onset time, at which the ordering and/or crystallization starts. The development of the transition showed a characteristic sigmoidal dependence on time for the samples. Furthermore, the curves in the bulk crystallization (DC_{18}DM-Br) exhibited much faster transition as compared with those of MMT-DC_{18}DM. The phase transition *half-time* $t_{1/2}$ with the reduced intensity reaches 1/2, and we defined $1/t_{1/2}$ as a measure of the overall transition rate at each characteristic curve in Fig. 9 (indicating the arrow), and plotted it in Fig. 10 against cooling rate. Interestingly, the estimated overall rate (0.40–4.35 s^{-1}) for MMT-DC_{18}DM coincides with the cooling rate in the range between 0.5 and 5.0 °C/min, beyond which they deviated to a downward trend. The downward deviation agreed well with the cooling rate dependence of T_c and ΔH_f (Fig. 8). In contrast, the DC_{18}DM-Br values showed a large value one order higher in magnitude as compared with those of MMT-DC_{18}DM, later reached a constant value (13.2 s^{-1}). The confined molecules (DC_{18}DMs) in one or two dimensional order exhibit significant contribution to enhance the nonisothermal phase transition (chain packing) at higher cooling rate (~5.0–20.0 °C/min) despite some downward deviation. As discussed above, this is presumably due to the poor chain packing for the ordered alkyl chains in MMT-DC_{18}DM.

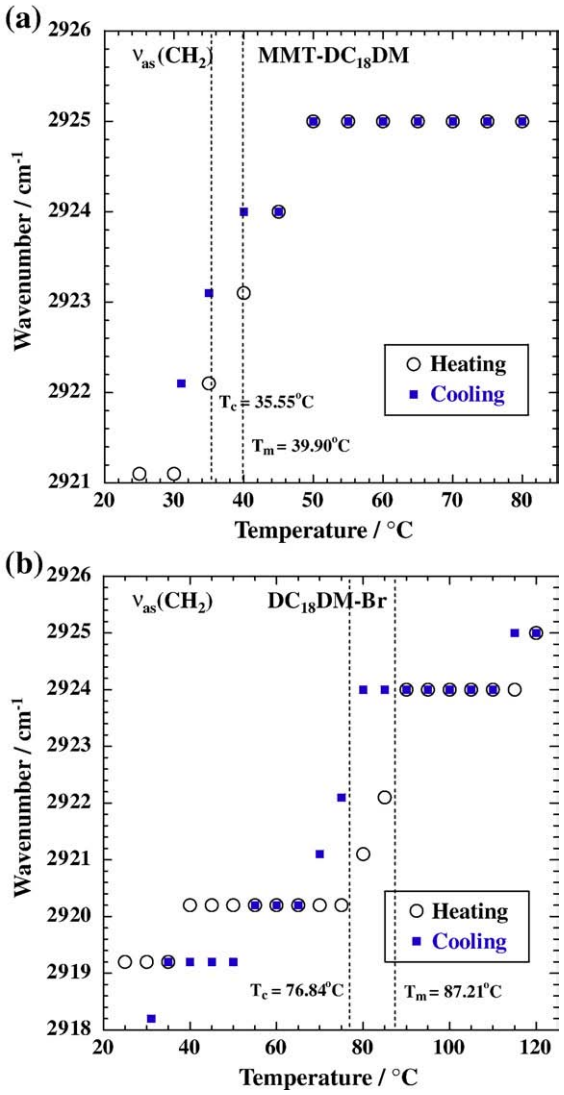

Fig. 6. Temperature variations of frequency shifts in the characteristic band ($\nu_{as}(CH_2)$) upon cyclic thermal treatment for (a) MMT-DC_{18}DM and (b) DC_{18}DM-Br. The dashed lines indicate T_c and T_m detected by TMDSC.

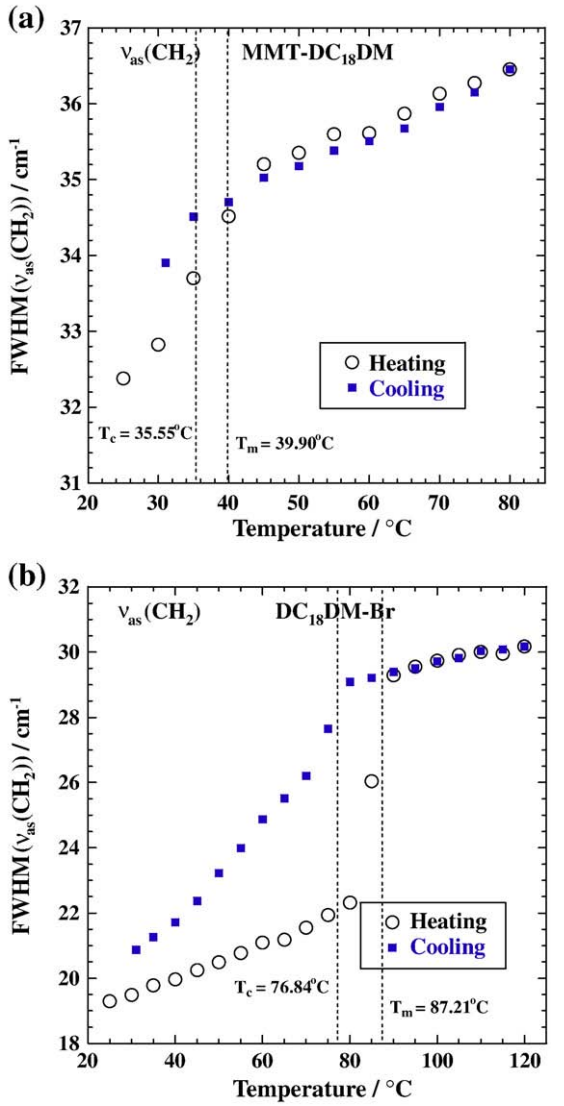

Fig. 7. Temperature variations of FWHM for the characteristic band ($\nu_{as}(CH_2)$) upon cyclic thermal treatment for (a) MMT-DC_{18}DM and (b) DC_{18}DM-Br. The dashed lines indicate T_c and T_m detected by TMDSC.

To confirm the ordering kinetics of the nonisothermal transition behavior of the cationic surfactants in MMT upon confinement, Arrhenius plot was constructed with the cooling rate *versus* reciprocal of the absolute phase transition (chain packing) temperature, $1/T_c$ as shown in Fig. 11.

The Ozawa–Flynn–Wall method based on Doyle's approximation (Ozawa, 1970; Moroni et al., 1986) can be used to find the effective activation energy and is expressed as follows:

$$Cooling\,rate \sim \exp(1.052E_a / RT_c) \quad (3)$$

where E_a is the activation energy for the nonisothermal phase transition, RT_c is the thermal energy. For both cases examined, the plots conformed to two straight lines in the different T_c regime. The slope that reflects the activation energy of the nonisothermal process was reduced when the cooling rate was beyond 5.0 °C/min. For example, in the polymer melt crystallization, the E_a value decreased upon increasing the crystallization temperature throughout both glass and melt crystallization regions (Vyazovkin and Dranca, 2006). In Fig. 11, similar changes are found at a cooling rate of 5.0 °C/min. This feature is superficially similar to the result as shown in Figs. 8 and 10. For MMT-DC_{18}DM, the significant change in E_a ($=947\pm5$ to 110 ± 20 kJ/mol) was found when compared with that of DC_{18}DM-Br ($E_a=535\pm5$ to 254 ± 12 kJ/mol, which is almost the same (~200–400 kJ/mol) in the polymer melt crystallization based on isoconversional analysis reported by Vyazovkin and Sbirrazzuoli (2006)). This indicates a possible change in the disorder–order phase transition mechanism. A significant decrease in E_a is correlated with the nonisothermal ordering associated with the poor chain packing of the alkyl chains and its molecular mobility in MMT-DC_{18}DM. In other words, the promoted chain packing in different T_c ranges (cooling rate >5.0 °C/min) showed much lower energy barrier ($E_a=110\pm20$ kJ/mol) as shown in Fig. 10.

Further studies are currently in progress to elucidate the effect of the molecular chain confinement and the significantly large negative Δp on the ordering process into the nano-galleries of MMT (Okamoto and Saito, in preparation).

4. Conclusions

We have examined the detailed nonisothermal ordering kinetics and disorder transition (chain melting) behavior including the conformational changes of the chain segment of the alkyl chains in the confined space (nano-gallery space in MMT). Chain packing and melting of the confined alkyl chains in MMT-DC_{18}DM are reversible

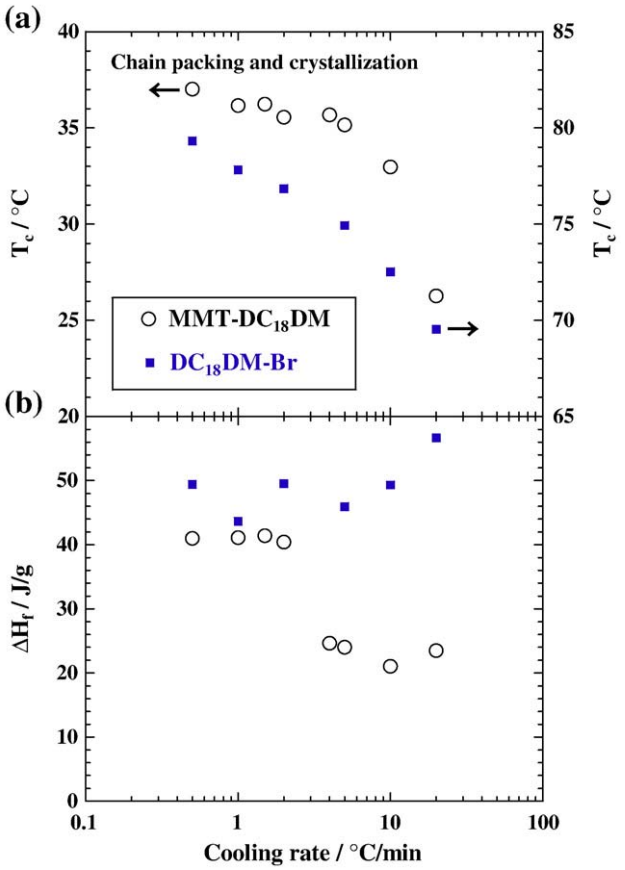

Fig. 8. Cooling rate dependence of (a) T_c and (b) ΔH_f for MMT-DC_{18}DM and DC_{18}DM-Br.

processes with some hysteresis owing to the difference between T_m and T_c. The formation of gauche conformers was enhanced and the poor chain packing took place for the alkyl chains in MMT-DC_{18}DM as compared with those of the crystallized DC_{18}DM-Br in bulk.

Via the order–disorder transition kinetic, it was found that the ordering in the confined space was more obvious as opposed to the bulk crystallization. For DC_{18}DM-Br, the overall crystallization rates exhibited large value one order higher in magnitude when compared

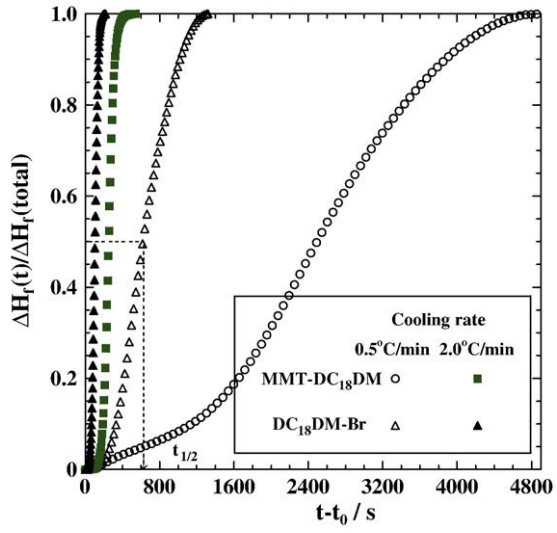

Fig. 9. Time variation of reduced degree of the degree of ordering ($\Delta H_f(t)/\Delta H_f$(total)) at two different cooling rate (0.5 and 2.0 °C/min). The dashed line indicates the phase transition half-time $t_{1/2}$.

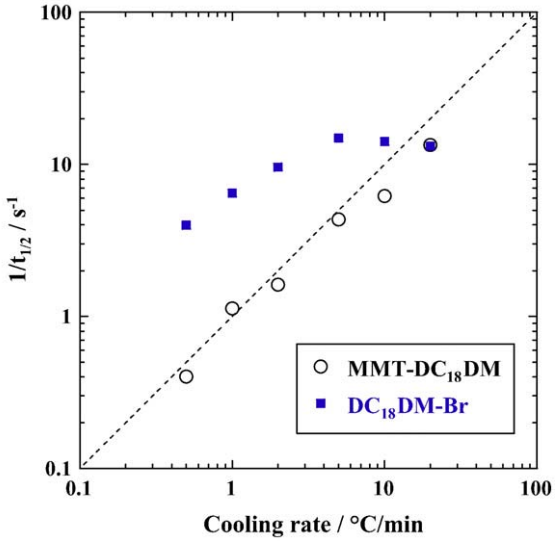

Fig. 10. Cooling rate dependence of overall phase transition rate ($1/t_{1/2}$). The dashed line indicates the linear relation between *x*- and *y*-axes.

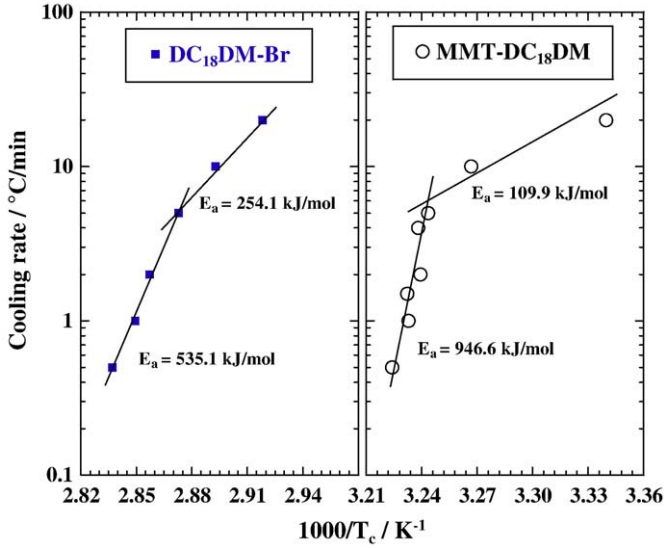

Fig. 11. Arrhenius plots of cooling rate *versus* reciprocal of the absolute phase transition temperature, $1/T_c$. The solid line is calculated by linear regression.

to MMT-DC_{18}DM. However, these values were strongly affected by the increase of the cooling rate and later achieved a constant value. The confined molecules (DC_{18}DMs) in one or two dimensional order exhibited significant contribution to enhance the nonisothermal ordering (chain packing) for a higher cooling rate.

Acknowledgment

This work was supported by KAKENHI (19656173) and the MEXT "Collaboration with Local Communities" Project (2005–2009).

References

Asai, K., Okamoto, M., Tashiro, K., 2008. Crystallization behavior of nano-composite based on poly(vinylidene fluoride) and organically modified layered titanate. Polymer 49, 4298–4306.

Bailey, S.W. (Ed.), 1988. Hydrous phyllosilicates: Reviews in Mineralogy, Mineralogical Society of America, Chelsea, MI, Vol. 19.

Binder, H., Kohlstrunk, B., Brenn, U., Schwieger, W., Klose, G., 1998. Infrared dichroism measurements on the alkyl chain packing of an ionic detergent intercalated between silicate layers. Colloid Polym. Sci. 276, 1098–1109.
Brovelli, D., Casei, W.R., Hähner, G., 1999. Self-assembled monolayers of alkylammonium ions on mica: direct determination of the orientation of the alkyl chains. J. Colloid Interface Sci. 216, 418–423.
Bunn, C.W., 1939. The crystal structure of long-chain normal paraffin hydrocarbons. The "shape" of the <CH2 group. Trans. Faraday Soc. 35, 482–491.
Fujii, M., Li, B., Fukuda, K., Kato, T., Seimiya, T., 1999. Heterogeneous growth and self-repairing processes of two-dimensional molecular aggregates of adsorbed octadecyltrimethylammonium bromide at cleaved mica/aqueous solution interface as observed by in situ atomic force microscopy. Langmuir. 15, 3689–3692.
Gao, F., 2004. Clay/polymer composites: the story. Materials Today 7, 50–55.
He, H., Galy, J., Gerard, J.F., 2005. Molecular simulation of the interlayer structure and the mobility of alkyl chains in HDTMA$^+$/montmorillonite hybrids. J. Phys. Chem. B. 109, 13301–13306.
Heinz, H., Castelijns, H.J., Suter, U.W., 2003. Structure and phase transitions of alkyl chains on mica. J. Am. Chem. Soc. 125, 9500–9510.
Heinz, H., Koerner, H., Anderson, K.L., Vaia, R.A., Farmer, B.L., 2005. Force field for mica-type silicates and dynamics of octadecylammonium chains grafted to montmorillonite. Chem. Mater. 17, 5658–5669.
Heinz, H., Vaia, R.A., Farmer, B.L., 2006. Interaction energy and surface reconstruction between sheets of layered silicates. J. Chem. Phys. 124, 224713–224719.
Heinz, H., Vaia, R.A., Krishnamoorti, R., Farmer, B.L., 2007. Self-assembly of alkylammonium chains on montmorillonite: effect of chain length, head group structure, and cation exchange capacity. Chem. Mater. 19, 59–68 Chelsea, MI.
Heinz, H., Vaia, R.A., Farmer, B.K., 2008. Relation between packing density and thermal transitions of alkyl chains on layered silicate and metal surfaces. Langnuir 24, 3727–3733.
Hussain, F., Hojjati, M., Okamoto, M., Gorga, R.E., 2006. Review paper: polymer–matrix nanocomposites, processing, manufacturing, and application: an overview. J. Composite Mater. 40, 1511–1575.
Krishnamoorti, R, Vaia, RA, Giannelis, EP, 1996. Chem. Mater 8, 1728–1734.
Kubo, H., Sato, H., Okamoto, M., Kotaka, T., 1998. Elongational flow opto-rheometry for polymeric liquids: 4. Rayleigh scattering studies on elongational flow-induced crystallization of poly(ethylene terephthalate) in the supercooled state. Polymer. 39, 501–503.
Lagaly, G., 1970. Layer charge determination by alkylammonium ions. Clays Clay Minerals. 16, 1–46.
Lagaly, G., Ogawa, M., Dekany, I., 2006. Clay mineral organic interactions. Handbook of Clay Science. Elsevier, Amsterdam, pp. 309–377. Chapter 7.3.
Li, Y., Ishida, H., 2002. A differential scanning calorimetry study of the assembly of hexadecylamine molecules in the nanoscale confined space of silicate galleries. Chem. Mater. 14, 1398–1404.
Li, Y., Ishida, H., 2003. Concentration-dependent conformation of alkyl tail in the nanoconfined space: hexadecylamine in the silicate galleries. Langnuir 19, 2479–2484.
Moroni, A., Mijovic, J., Pearce, E., Foun, C.C., 1986. Cure kinetics of epoxy resins and aromatic diamines. J. Appl. Polym. Sci. 32, 3761–3773.
Nuzzo, R.G., Dubois, L.H., Allara, D.L., 1990. Fundamental studies of microscopic wetting on organic surfaces. 1. Formation and structural characterization of a self-consistent series of polyfunctional organic monolayers. J. Am. Chem. Soc. 112, 558–569.
Okada, A., Usuki, A., 2006. Twenty years of polymer–clay nanocomposites. Macromol. Mater. Eng. 291, 1449–1476.
Okamoto M, Saito T, in preparation.
Okamoto, M., Taguchi, H., Sato, H., Kotaka, T., Tateyama, H., 2000. Dispersed structure and rheology of lipophilized-smectite/toluene suspensions. Langumuir 16, 4055–4058.
Osman, M.A., Seyfang, G., Suter, U.W., 2000. Two-dimensional melting of alkane monolayers ionically bonded to mica. J. Phys. Chem. B. 104, 4433–4439.
Osman, M.A., Ernst, M., Meier, B.H., Suter, U.W., 2002. Structure and molecular dynamics of alkane monolayers self-assembled on mica platelets. J. Phys. Chem. B. 106, 653–662.
Osman, M.A., Ploetze, M., Skrabl, P., 2004. Structure and properties of alkylammonium monolayers self-assembled on montmorillonite platelets. J. Phys. Chem. B. 108, 2580–2588.
Ozawa, T., 1970. Kinetic analysis of derivative curves in thermal analysis. J. Therm. Anal. Calorim. 2, 301–324.
Rao, Y., Pochan, J.M., 2007. Mechanics of polymer–clay nanocomposites. Macromolecules 40, 290–296.
Sinha Ray, S., Okamoto, M., 2003. Polymer/layered silicate nanocomposites: a review from preparation to processing. Prog. Polym. Sci. 28, 1539–1641.
Vaia, R.A., Giannelis, E.P., 1997a. Polymer melt intercalation in organically-modified layered silicates: model predictions and experiment. Macromolecules 30, 8000–8009.
Vaia, R.A., Giannelis, E.P., 1997b. Lattice model of polymer melt intercalation in organically-modified layered silicates. Macromolecules 30, 7990–7999.
Vaia, R.A., Wagner, H.D., 2004. Framework for nanocomposites. Materials Today 7, 32–37.
Vaia, R.A., Teukolsky, R.K., Giannelis, E.P., 1994. Interlayer structure and molecular environment of alkylammonium layered silicates. Chem. Mater. 6, 1017–1022.
Vyazovkin, S., Dranca, I., 2006. Isoconversional analysis of combined melt and glass crystallization data. Macromole. Chem. Phys. 20, 20–25.
Vyazovkin, S., Sbirrazzuoli, N., 2006. Isoconversional kinetic analysis of thermally stimulated processes in polymers. Macromol. Rapid Commun. 27, 1515–1532.
Yoshida, O., Okamoto, M., 2006a. Direct melt intercalation of polylactide chains into nano-galleries: interlayer expansion and nanocomposite structure. Macromole. Rappid Commun. 27, 751–757.
Yoshida, O., Okamoto, M., 2006b. Direct melt intercalation of polymer chains into nano-galleries: interdigitated layer structure and interlayer expansion. J. Polym. Eng. 26, 919–939.